ELSEVIER

Polymer 41 (2000) 6271–6283

polymer

High-energy mechanical milling of poly(methyl methacrylate), polyisoprene and poly(ethylene-*alt*-propylene)

A.P. Smith[a,1], J.S. Shay[b], R.J. Spontak[a,b,*], C.M. Balik[a], H. Ade[c], S.D. Smith[d], C.C. Koch[a]

[a]*Department of Materials Science and Engineering, North Carolina State University, Raleigh, NC 27695, USA*
[b]*Department of Chemical Engineering, North Carolina State University, Raleigh, NC 27695, USA*
[c]*Department of Physics, North Carolina State University, Raleigh, NC 27695, USA*
[d]*Corporate Research Division, The Procter and Gamble Company, Cincinnati, OH 45239, USA*

Received 4 August 1999; received in revised form 4 November 1999; accepted 5 November 1999

Abstract

High-energy mechanical milling has been performed on poly(methyl methacrylate) (PMMA) at ambient and cryogenic temperatures, as well as on polyisoprene (PI) and poly(ethylene-*alt*-propylene) (PEP) at cryogenic conditions only. Milling conducted at ambient temperature has a substantially greater impact on the molecular characteristics of PMMA than milling at cryogenic temperatures. An increase in the milling time is accompanied by substantial reductions in PMMA molecular weight and, hence, glass transition temperature and impact strength under both sets of experimental conditions. An unexpected trend identified here is that the PMMA molecular weight distribution initially broadens and subsequently narrows with increasing milling time. Solid-state mechanical milling promotes comparable decreases in molecular weight and glass transition temperature in PEP (at a slower rate relative to PMMA), but induces chemical crosslinking in PI, as confirmed by FTIR spectroscopy. Charlesby–Pinner analysis yields not only the degree of PI crosslinking, but also the relative crosslinking and scission rates of PI, during cryogenic milling.

Keywords: Mechanical milling; Mechanical attrition; Glass transition temperature

1. Introduction

Without a doubt, the most significant impediment to producing intimately (nanoscale) mixed blends of dissimilar polymeric materials lies in the intrinsic immiscibility of macromolecules [1,2]. In most conventional processes, polymers are blended in a fashion that endows the chains with sufficient mobility for the constituent polymer species to phase-separate, which is often accompanied by severe degradation of thermal, optical and/or mechanical properties. Since most high-throughput blending techniques rely on melt or solution processing, numerous studies continue to explore physical and reactive compatibilization routes as methods which promote (and retain) intimate polymer dispersion during processing [3–6]. An alternative strategy for producing polymer blends, while avoiding the problem of phase separation, relies on solid-state mixing, which generally involves the efficient grinding of two or more polymer species [2]. Mechanical action can, however, have deleterious effects on polymers in the solid (glassy or crystalline) state by breaking chains and creating free radicals. For this reason, high-dispersion solid-state blending is only now being realized as a viable technology. Recent years have witnessed resurgence in this process through the increased use of mechanical ball milling [7–11] and solid-state extrusion pulverization [12,13] in preparing polymer blends. The objective of the present work is to explore the effects of high-energy mechanical milling on the molecular and physical properties of single homopolymers, since a fundamental understanding of these effects is prerequisite to the use of mechanical alloying as a means of producing novel polymer blends.

Mechanical milling (involving one material) and mechanical alloying (involving two or more materials) generally refer to high-energy ball-milling techniques employed to process materials in the solid state [14]. These non-equilibrium processing routes, responsible for the early successes in oxide dispersion strengthening of metallic superalloys [15], have expedited production of a wide variety of metastable inorganic materials and morphologies (both single component and alloys), and are

* Corresponding author. Tel.: +1-919-515-4200; fax: +1-919-515-7724.
E-mail address: rich_spontak@ncsu.edu (R.J. Spontak).
[1] Present address: Polymers Division, National Institute of Standards and Technology, Gaithersburg, MD 20899, USA.

0032-3861/00/$ - see front matter
PII: S0032-3861(99)00830-7

Table 1
Molecular characteristics of the as-received polymers employed in this study

Sample designation	Reported $\bar{M}_w$ (kg mol^{-1})	Measured $\bar{M}_w$ (kg mol^{-1})	Measured $\bar{M}_n$ (kg mol^{-1})	PDI
h-PMMA	996	1040	255	4.08
m-PMMA	120	121	67.1	1.80
l-PMMA	15	16.6	14.8	1.12
n-PMMA	100	92.0	73.8	1.25
PI	60	72.1	68.8	1.05
PEP[a]	60	67.1	63.4	1.06

[a] The difference in molecular weight characteristics between PI and PEP is due to their different hydrodynamic volumes.

presently used to form extended solid solutions, novel intermediate phases, alloys from immiscible metals and oxides, metal–ceramic composites and nanocrystalline materials [14,16,17]. Application of high-energy mechanical milling to polymeric materials, however, remains relatively recent, initiated by Shaw and co-workers in the early 1990s [7,8,18,19]. These and subsequent [9–11,20] investigations have focused primarily on milling-induced structural and property changes in semi-crystalline polymers and their blends, but have not elucidated, in systematic fashion, the molecular physico-chemical changes that occur as a result of milling.

Prior works addressing the mechanochemistry of polymers have often sought to identify and explain the stress-induced molecular changes that arise in molten or solvated polymers during the course of mechanical processes such as grinding, extruding and stirring [21–24]. Issues regarding, for instance, changes in molecular weight and molecular weight distribution, as well as free-radical generation and mechanisms, have received considerable attention in this vein. Although induced by different means, the physico-chemical changes of macromolecules due to mechanical milling are expected to be similar to those incurred by these related mechanical processes. A complex combination of shearing, extension, fracture and cold-welding of polymer powder particles during milling may induce chain scission or hydrogen abstraction and generate free radicals. While chain scission would be accompanied by a reduction in molecular weight, it is conceivable that free radicals may promote interchain reactions and, hence, chemical crosslinking.

Modification of a single polymer or a polymer blend by high-energy mechanical milling is therefore anticipated to have a profound effect on the properties of polymeric material(s) in a relatively unpredictable manner. In a recent investigation [25] of poly(ethylene terephthalate) (PET) mechanically milled at ambient and cryogenic temperatures, for example, milling is found to promote amorphism in both high- and low-crystallinity PET. Within this metastable state, the PET chains are highly aligned to form an almost nematic mesophase. Upon post-annealing, the chains readily form crystals, thereby demonstrating that milling has a profound impact on molecular alignment and structure development in some thermoplastic polymers. In the present study, we employ molecular weight (M), glass transition temperature (T_g) and impact strength measurements to probe the time-dependent molecular and property evolution of three homopolymers—poly(methyl methacrylate) (PMMA), polyisoprene (PI) and poly(ethylene-*alt*-propylene) (PEP)—during high-energy mechanical milling in the solid state.

2. Experimental

2.1. Materials

Three grades of PMMA differing in number- and weight-average molecular weight ($\bar{M}_n$ and $\bar{M}_w$, respectively) were purchased from Aldrich and used as-received. In addition, another PMMA homopolymer, as well as a PI homopolymer and its hydrogenated PEP analog were custom-synthesized via living anionic polymerization. The molecular weight characteristics of these six materials, as discerned by gel permeation chromatography (GPC), and their designations are listed in Table 1. The PMMA homopolymers were milled at ambient temperature (*ambi*milled) and liquid nitrogen temperature (*cryo*milled), whereas the PI and PEP homopolymers were only subjected to cryomilling due to their low T_gs. In all cases, 3 g of polymer were placed in a hardened steel vial (about 60 ml full capacity) with 30 g of steel ball bearings (6.4 and 7.9 mm in diameter), and the vial was sealed under Ar (with <10 ppm of O_2). For ambi-milling experiments, the sealed vial was placed in a standard SPEX 8000 mill and violently agitated at 20 Hz without any coolant (the external vial temperature remained at 30°C). For cryomilling experiments, the vial was placed in a custom-designed nylon sleeve designed to allow peripheral flow of liquid nitrogen and, hence, maintain a constant external vial temperature (at ca. -180°C) during milling. The vial assembly was placed in a modified SPEX 8000 mill (reinforced to handle the extra mass and torque applied during operation) and vigorously shaken. Specimens were milled for intervals up to 10 h, after which time fine powders were removed and stored.

2.2. Methods

The thermal properties of the milled polymers were

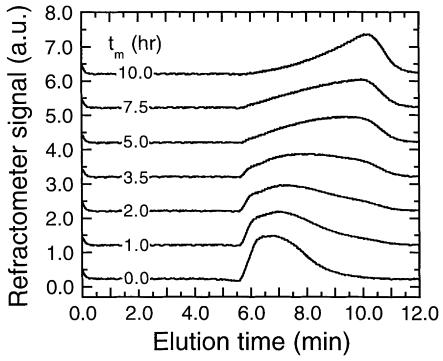

Fig. 1. Gel permeation chromatograms of h-PMMA cryomilled for different times (t_m, shown in the figure) indicating that the PMMA molecular weight decreases with increasing t_m. Note that the distribution initially broadens but eventually narrows, indicating preferential scission of long chains. The chromatograms displayed here are shifted vertically to facilitate comparison.

characterized by differential scanning calorimetry (DSC) with a DuPont Instruments 910 calorimeter, operated at a heating rate of 20°C min^{-1} under an Ar purge. Molecular weight measurements were performed as a function of milling time (t_m) by GPC with a Waters 2690 injection unit and Styragel® HR4 columns. Light scattering and differential pressure measurements were concurrently performed at ambient temperature from 10 mg ml^{-1} polymer solutions in THF (100 μl injections at a flow rate of 1 ml min^{-1}) with a Wyatt Technology Interferometric Refractometer and a Viscotek T60A dual detector, respectively. Sol–gel analysis was conducted by vacuum-assisted filtration on cryomilled PI (0.4 wt% in toluene) using Fisher quantitative filter paper Q2 (particle retention <1 μm). Fourier-transform infrared (FTIR) spectroscopy was performed on cryomilled PI from 400 to 4000 cm^{-1} (at a resolution of 2 cm^{-1}) with a Nicolet Magna-IR Spectrometer 750 equipped with an attenuated total reflectance (ATR) cell and a ZnSe crystal. All non-calorimetric measurements were performed at ambient temperatures.

The impact strength of milled PMMA specimens was measured at 25°C on a Tinius-Olsen 92T impact tester modified to accept short (10 mm) samples. Impact samples were prepared by compacting ca. 1.6 g of powder to a disk 25 mm in diameter at ambient temperature and 88 MPa for 5 min. These disks were next melt-pressed into squares with minimal pressure at a temperature 40°C above the measured T_g of the powder (ranging from 100 to 160°C, depending on t_m) for 5 min, then quenched to ambient temperature in water. The squares were 2 mm thick and 25.4 mm on a side, and were subsequently cut into "matchsticks" measuring 2 mm × 4 mm × 25 mm with a Buehler Isomat diamond saw. Each matchstick was placed 5 mm into the clamp of the impact tester and oriented such that the striker hit the 2 mm side and fracture occurred along the 4 mm side. The matchsticks were not notched. A torque of 60 N-cm was applied to the clamp, which exerted a force of 330 N. After initial fracture, the remaining part of the matchstick

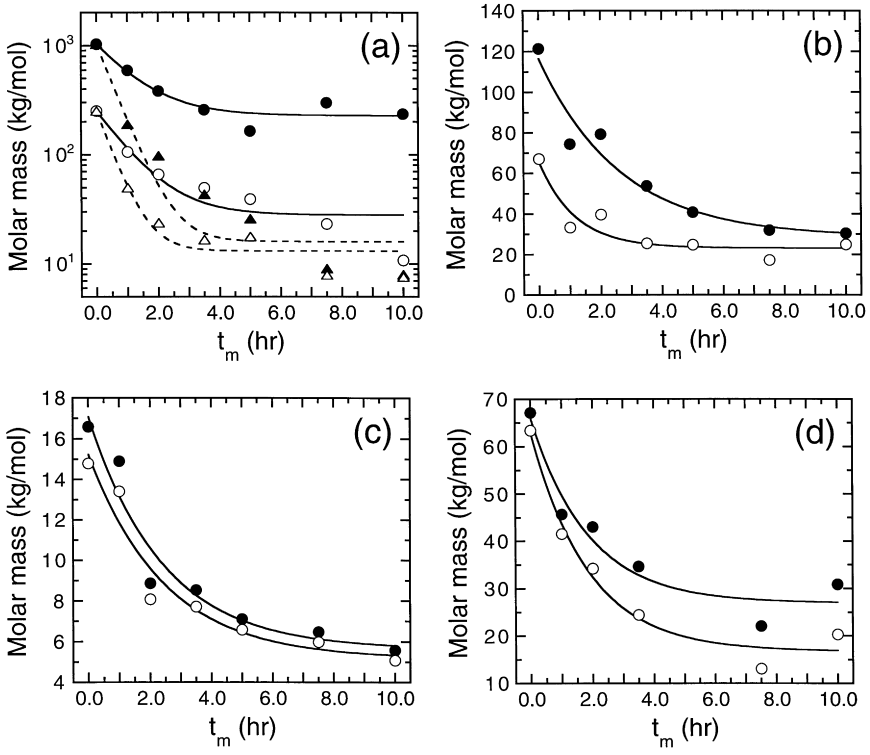

Fig. 2. Dependence of $\bar{M}_n$ (open symbols) and $\bar{M}_w$ (filled symbols) on t_m for: (a) h-PMMA subjected to cryomilling (circles, solid lines) and ambimilling (triangles, dashed lines); (b) cryomilled m-PMMA; (c) cryomilled l-PMMA; and (d) cryomilled PEP. The lines correspond to regressed fits of Eq. (1) in the text, and resulting parameters are included in Table 3.

Table 2
Measured polydispersity indices of PMMA and PEP as a function of milling time

t_m (h)	h-PMMA (cryomilled)	h-PMMA (ambimilled)	m-PMMA	l-PMMA	n-PMMA	PEP
0.0	4.08	4.08	1.80	1.12	1.25	1.06
1.0	5.61	3.81	2.23	1.11	1.78	1.10
2.0	5.83	4.11	2.22	1.10	2.16	1.26
3.5	5.21	2.60	2.12	1.11	1.56	1.41
5.0	4.21	1.45	1.65	1.08	1.35	1.25
7.5	12.87	1.14	1.86	1.08	–	1.69
10	21.82	1.05	1.22	1.10	–	1.52

was subjected to impact testing twice more until it became too short for testing. About 15 measurements were acquired from each specimen, and as many as two outlying measurements were discarded per specimen.

3. Results and discussion

3.1. Molecular weight

To ascertain the effect of high-energy mechanical milling on the molecular weight distribution of each homopolymer examined here, GPC was performed on solutions of the as-milled materials in THF. Fig. 1 shows a set of concentration curves obtained for h-PMMA cryomilled for different t_m up to 10 h. The data presented in Fig. 1 represent the output signal from the refractometer and are scaled and offset to facilitate comparison. According to the data tabulated in Table 1, the h-PMMA polymer possesses a relatively high target molecular weight and polydispersity index (PDI = $\bar{M}_w/\bar{M}_n$). Upon mechanical milling, the peak in the chromatogram from the as-received material initially becomes less intense, and then broadens and shifts to longer retention times with increasing t_m. Eventually, however, the peak begins to intensify and, once again, becomes relatively narrow at long t_m. These results reveal two important trends: (i) the molecular weight of h-PMMA decreases with increasing t_m; and (ii) the molecular weight distribution initially broadens before narrowing as low-molecular-weight chains are produced during milling.

Calculated values of $\bar{M}_n$ and $\bar{M}_w$ derived from GPC traces such as those provided in Fig. 1 are displayed as a function of t_m in Fig. 2 for h-PMMA (Fig. 2a), m-PMMA (Fig. 2b), l-PMMA (Fig. 2c) and PEP (Fig. 2d). In all cases, both average molecular weights are observed to decrease substantially with increasing t_m, with the magnitude of reduction varying from a factor of 2 (PEP) to a factor of 130 (ambimilled h-PMMA). Results obtained for both cryomilled and ambimilled h-PMMA are included for comparison in Fig. 2a and reveal that ambimilling yields a much more pronounced reduction in molecular weight than cryomilling. Corresponding PDI values, provided in Table 2, initially increase with increasing t_m in both series, but remain large (PDI $>$ 4.08) for cryomilled h-PMMA. In marked contrast, ambimilling eventually yields a nearly monodisperse molecular weight distribution (PDI = 1.05) at the cost of an extremely depressed molecular weight ($\bar{M}_w = 7.99$ kg mol^{-1}), in h-PMMA. Comparable behavior is observed for cryomilled m-PMMA (Fig. 2b), viz. the PDI initially increases before decreasing with increasing t_m, without such a dramatic decline in molecular weight. For cryomilled l-PMMA (Fig. 2c), both $\bar{M}_n$ and $\bar{M}_w$ are seen to decrease at similar rates with respect to t_m (a factor of about three reduction in each is achieved after 10 h of cryomilling), indicating that the polydispersity in this material remains nearly constant with t_m. It is of interest to note that the $\bar{M}_n$ and $\bar{M}_w$ values obtained from h-PMMA and m-PMMA cease decaying at values higher than the initial values of m-PMMA and l-PMMA, respectively. This indicates that the milled PMMA possesses intrinsically different behavior relative to the unmilled polymer when subjected to extended milling.

The cryomilling-induced changes in molecular weight recorded for PEP are presented in Fig. 2d and clearly do not follow the trends described above for PMMA. For this homopolymer, the molecular weight decreases by a factor of 2–3 at $t_m = 10$ h, but the polydispersity continues to increase monotonically with increasing t_m (see Table 2). Since the rate of molecular weight reduction appears to be significantly slower for PEP than for PMMA, it is possible that, on one hand, PDI convergence may simply not have been attained during the course of t_m examined. On the other hand, this disparity in the milling-induced evolution of molecular weight distribution may reflect a fundamental difference between the physico-chemical responses of PEP and PMMA to solid-state milling. Additional analysis in this vein with the PI homopolymer is, unfortunately, not possible due to the insolubility of cryomilled PI, which precludes GPC analysis. This observation is discussed further later in this work.

One approach by which the molecular weight trends evident in Fig. 2 can be analyzed has been suggested by Baramboim [21], who explored the molecular weight degradation of polymers subjected to mechanical processing. In this analysis, the time-dependent molecular weight of a polymer is given by

$$M(t_m) = M_\infty + a\, e^{-kt_m} \quad (1)$$

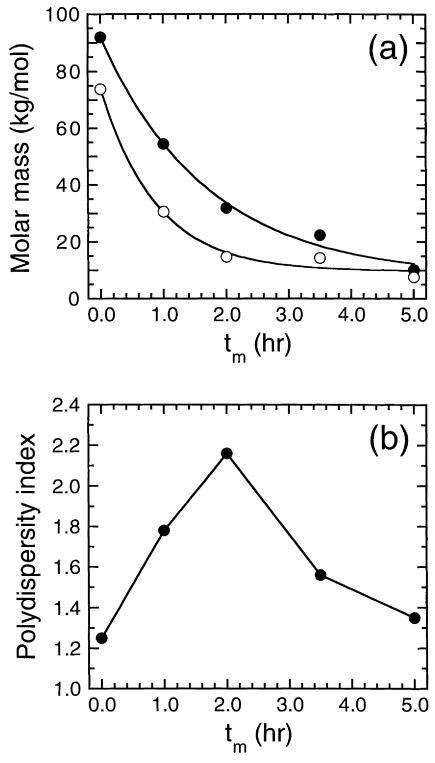

Fig. 3. Variation of (a) $\bar{M}_n$ (○) and $\bar{M}_w$ (●) and (b) the PDI with t_m for n-PMMA, which possesses an initially narrow molecular weight distribution (PDI = 1.24). Note that the PDI initially increases and subsequently decreases with increasing t_m.

where M_∞ denotes the molecular weight of the polymer that cannot be reduced further, a is a constant and k represents a degradation constant, which is sensitive to the milling parameters, as well as to polymer chemistry and chain conformation. Provided in Table 3 are values of M_∞ and k discerned from a non-linear least-squares fit of Eq. (1) to the $\bar{M}_n$ data in Fig. 2. To place these values in perspective, Baramboim [21] reports $M_\infty = 9.0$ kg mol^{-1} and $k = 0.12$ h^{-1} for PMMA subjected to a mechanical process that is not explicitly detailed. Thus, the values deduced for k in this work are generally (and markedly) higher than those reported elsewhere, indicating that mechanical milling is a much higher energy technique than the one employed by Baramboim [21].

Examination of the data in Table 3 yields several important conclusions. First, the values of M_∞ and k differ depending on initial PMMA molecular weight and milling temperature (ambimilled versus cryomilled). Both M_∞ and k appear to increase non-linearly with increasing $\bar{M}_n$ (or, alternatively, $\bar{M}_w$) of the unmilled PMMA. Similar variation of M_∞ with initial polymer molecular weight has been previously observed [22] in mechanically processed systems. Furthermore, values of M_∞ and k for the h-PMMA and m-PMMA homopolymers are comparable in magnitude. Such similarity may not be surprising since both h-PMMA and m-PMMA possess initial $\bar{M}_n$ values far in excess of the critical molecular weight of entanglement ($M_c = 27.5$ kg mol^{-1}) for PMMA [26,27]. In the present study, it is interesting to note that, in the PMMA homopolymers initially with $\bar{M}_n > M_c$, M_∞ only differs from M_c by as much as about 15% (for h-PMMA), suggesting that cryomilling may not shorten long, entangled PMMA molecules below the limit of molecular entanglement.

Here, we return to the observation made earlier concerning the initial broadening and subsequent narrowing of the PMMA molecular weight distribution. This trend can be attributed to the high probability of preferentially breaking long molecules at short t_m and the generally lower probability associated with breaking short chains [21,22]. While the molecular weight and PDI data presented so far are consistent with this explanation, the PDI values of the initial (unmilled) h-PMMA and m-PMMA homopolymers are excessively high (4.08 and 1.80, respectively) to confirm this conclusion. This explanation can be tested more rigorously through the use of the PMMA homopolymer with $\bar{M}_n > M_c$ and a relatively low PDI (designated in Table 1 as n-PMMA). The time evolution of molecular weight and polydispersity in this homopolymer is shown in Fig. 3 for ambimilling times up to 5 h. Inspection of this figure reveals similar trends as those previously observed for the initially polydisperse PMMA homopolymers: (i) a sharp reduction in molecular weight by approximately an order of magnitude at short t_m; and (ii) an initial increase in PDI, followed by a comparable decrease (with a maximum PDI observed in the vicinity of $t_m = 2$ h). Fig. 3 therefore confirms the preferential breaking of long PMMA chains during the collisions that occur in high-energy mechanical milling at ambient or cryogenic temperatures.

Another trend evident from the data listed in Table 3 is that ambimilling PMMA yields a lower M_∞, but higher k (by almost a factor of two), than cryomilling, indicating that

Table 3
Regressed parameters derived for several polymers upon mechanical milling

Sample designation (process)	M_∞ (kg mol^{-1})	k (h^{-1})	T_g^∞ (°C)	$\alpha \times 10^{-5}$ (kg °C mol^{-1})
h-PMMA (cryomilled)	27	0.93	123.2	8.54
h-PMMA (ambimilled)	13	1.83	122.4	7.07
m-PMMA (cryomilled)	23	0.86	123.0	13.0
l-PMMA (cryomilled)	5.1	0.41	–	–
n-PMMA (ambimilled)	9.6	1.14	–	–
PEP (cryomilled)	20	0.54	–	–

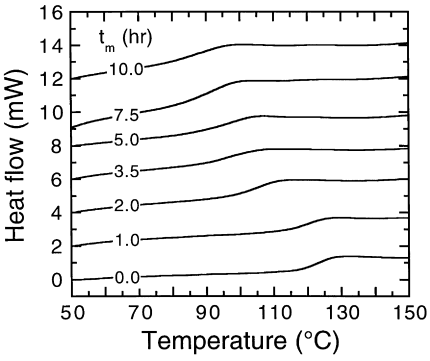

Fig. 4. Differential scanning calorimetry thermograms of h-PMMA subjected to cryomilling for different milling times (t_m, shown in the figure). These are all second-heat traces acquired at 20°C min^{-1} under Ar (first-heat data include distracting stress-related thermal responses).

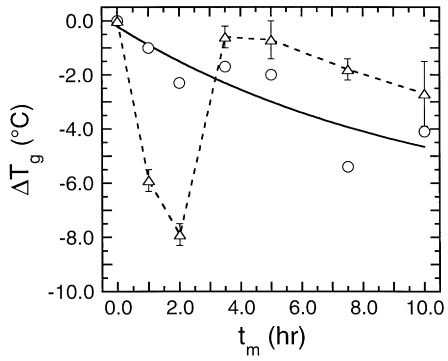

Fig. 6. Dependence of ΔT_g on t_m for cryomilled PEP (○) and PI (△). While PEP exhibits the same response as PMMA to increasing t_m (see Fig. 5), the change in ΔT_g for PEP occurs more slowly. Note that the time-dependent behavior of PI differs markedly from PMMA and PEP. The error bars denote one standard deviation in the data and provide a measure of reproducibility.

ambimilling causes more molecular degradation than cryomilling. This result may be somewhat counterintuitive, since polymer chains are anticipated to become increasingly embrittled with decreasing temperature. Previous studies have, however, reported that mechanical degradation increases substantially with decreasing temperature above T_g, but increases with increasing temperature below T_g [21,28]. In both ambimilling and cryomilling, the vial temperatures are well below the T_g of PMMA. The internal temperature rise, instantaneously fluctuating due to the high-energy collisions of the ball bearings, is not known with any degree of precision. Theoretical and experimental estimates of the local temperature increase (derived from milling-induced structural changes in inorganic materials) suggest that the increase can range from 10 to 400°C, depending primarily on mill type. For the SPEX mill employed here, however, an increase of less than 50°C is expected [17]. Since molecular weight degradation is more pronounced in the ambimilled PMMA relative to its cryomilled analog, PMMA most likely remains in its glassy state during both ambimilling and cryomilling. If, however, the local temperature increase became sufficiently high to heat the polymer above its T_g, the rate of chain damage at a given t_m due to ambimilling would be less than that due to cryomilling (assuming negligible thermo-oxidative effects) [21,28].

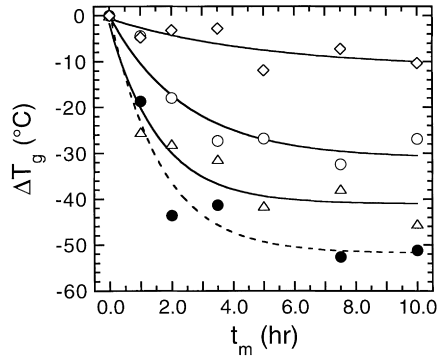

Fig. 5. Glass transition temperature shift, $\Delta T_g = T_g(t_m) - T_{g,0}$, presented as a function of t_m for cryomilled h-PMMA (○), ambimilled h-PMMA (●), m-PMMA (△) and l-PMMA (◇). The lines (solid for cryomilled samples and dashed for ambimilled samples) serve as guides for the eye.

The explanation for enhanced molecular weight reduction due to ambimilling relative to cryomilling lies in the thermodynamics of chain scission. In the case of mechanical degradation in the solid state, the activation energy required to break molecular bonds is supplied by an external stress applied to a polymer chain. The normal thermal vibrations of the atoms comprising the chain augment this stress. For a given stress state, it is therefore possible for a bond to be stable at one temperature, but unstable at a higher temperature [24]. Since the temperature difference between ambimilling and cryomilling in the present study is approximately 200°C, a much higher stress is required for chain scission during cryomilling relative to ambimilling. From the results obtained here, it can be concluded that mechanical milling of PMMA becomes increasingly more efficient with increasing temperature insofar as the PMMA remains in the solid (glassy) state. Comparable behavior has also been observed in the mechanical milling of PET [25] and polystyrene (data not shown), and may constitute a general response of thermoplastics to high-energy milling.

3.2. Glass transition temperature

According to the data presented in the previous section, mechanical milling has a significant impact on the molecular weight of PMMA and PEP. It is therefore reasonable to expect that M-dependent properties of these materials will likewise be affected. A thermal property that is sensitive to molecular weight is T_g, which for nearly monomolecular linear polymers can be conveniently written as [29,30]

$$T_g = T_g^{\infty} - \alpha \bar{M}_n^{-1} \quad (2)$$

Here, T_g^{∞} denotes the T_g in the limit as $\bar{M}_n \rightarrow \infty$ (which is valid in the mean-field limit) and α is a polymer-specific

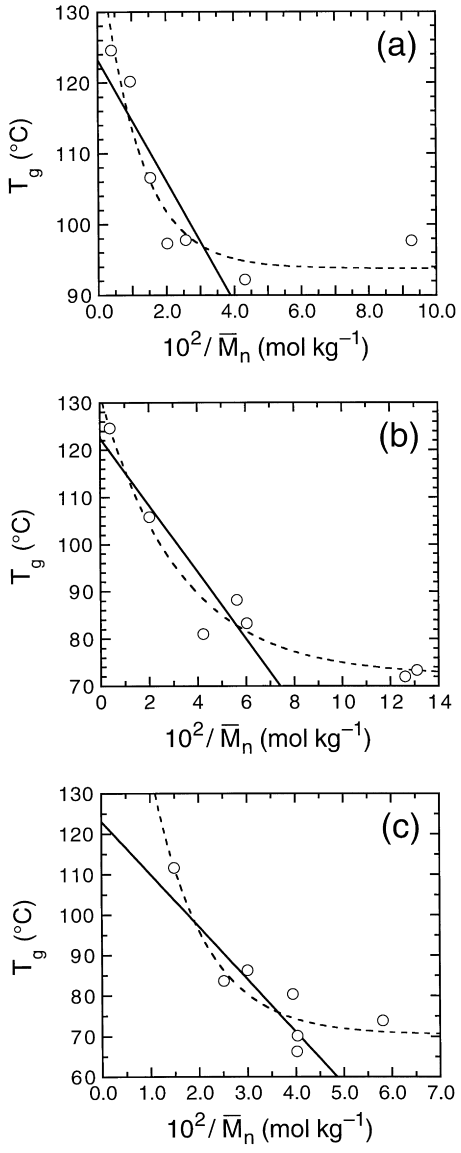

Fig. 7. Glass transition temperature presented as a function of $\bar{M}_n^{-1}$ for (a) cryomilled h-PMMA, (b) ambimilled h-PMMA; and (c) m-PMMA. A linear least-squares fit of Eq. (1) in the text (solid line) to each data set at short t_m yields the values of T_g^∞ and α listed in Table 3. The data are more accurately represented through the use of Eq. (3) in the text (dashed line).

constant. To ascertain the effect of high-energy mechanical milling on T_g, DSC thermograms have been acquired from all of the as-milled polymers and are displayed for cryomilled h-PMMA in Fig. 4. Note that these thermograms correspond to second heating scans, since the first scans (not shown here) exhibit distracting stress-related features (the focus of this section is on the milling-induced M-dependence of T_g). Examination of the thermograms in Fig. 4, which are illustrative of the m-PMMA and l-PMMA homopolymers, reveals that the T_g of the h-PMMA sample decreases, and that the T_g transition broadens markedly, with increasing t_m.

Analysis of thermograms such as those in Fig. 4 to extract midpoint T_gs yields the results presented in Fig. 5. In this figure, ΔT_g, defined as $T_g(t_m) - T_{g,0}$ where $T_{g,0}$ denotes the T_g of the unmilled polymer, is provided as a function of t_m for both cryomilled and ambimilled h-PMMA, ($T_{g,0} = 125$°C), cryomilled m-PMMA ($T_{g,0} = 112$°C) and cryomilled l-PMMA ($T_{g,0} = 94$°C). In all cases, a decrease in T_g (by as much as ca. 50°C) is observed as t_m is increased. This figure also shows that the milling-induced decrease in PMMA T_g is not a simple function of molecular weight in the cryomilled PMMA series, since the maximum T_g reduction beyond $t_m = 5$ h occurs in order (from highest to lowest) in m-PMMA, h-PMMA and l-PMMA. A possible explanation for this order is that the h-PMMA homopolymer possesses a very high PDI (4.08), whereas those of m-PMMA and l-PMMA are less than 2.00. In addition, the milling temperature is seen to have a substantial impact on T_g, with ambimilling promoting a much larger drop in the T_g of h-PMMA than cryomilling (ca. 50°C versus 30°C, respectively). This observation is consistent with the more pronounced effect of ambimilling on h-PMMA molecular weight degradation. It should be recognized that, if the reduction in T_g is sufficient, local heating generated during ambimilling may cause the h-PMMA to behave as a melt. Recall that the susceptibility of molten polymer chains to break during high-energy ball milling differs markedly from that of chains frozen in the solid state [21,28].

Fig. 6 shows the time-dependent variation of ΔT_g for PI and PEP, for which the values of $T_{g,0}$ are equal to -55.5 and -51.7°C, respectively. The cryomilled PEP is seen to emulate the same behavior recorded for the PMMA samples in Fig. 5, although it is unclear from the data in Fig. 6 whether a limiting value of ΔT_g has been reached after $t_m = 10$ h. An interesting difference between the data for PMMA and PEP in Figs. 5 and 6, respectively, is that the magnitude of ΔT_g is consistently smaller for PEP. In marked contrast, cryomilled PI does not even exhibit an initially monotonic reduction in ΔT_g. Instead, $\Delta T_g(t_m)$ attains a sharp minimum at a relatively short t_m (2 h) and subsequently increases almost back to zero, decreasing slightly from zero (by about 2.7°C at $t_m = 10$ h) thereafter. This behavior, which is completely reproducible (as evidenced by the error bars included in Fig. 6) is indicative that cryomilling affects PI differently relative to PMMA and PEP. Recall from the previous section that the molecular weight distribution of PI could not be measured by GPC due to insolubility of cryomilled PI in the carrier solvent. The sharp increase in the T_g (or, alternatively, ΔT_g in Fig. 6) of cryomilled PI after $t_m = 2$ h, accompanied by its apparent insolubility, strongly suggests that the PI chains undergo chemical crosslinking during cryomilling. In this case, we envisage a highly dynamic competition between chains breaking (causing a decrease in molecular weight) and crosslinking (promoting an increase in molecular weight) under highly non-equilibrium conditions. We return to this topic in the final section of this study.

As indicated by Eq. (2), T_g can depend sensitively on $\bar{M}_n$ when $\bar{M}_n$ becomes relatively small, as is the case here. The

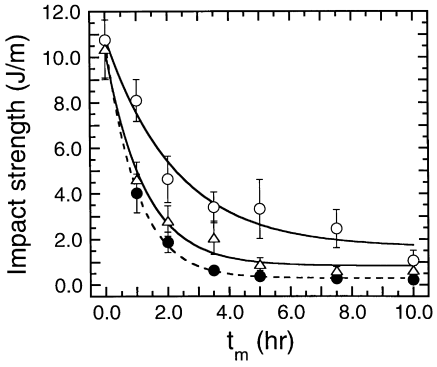

Fig. 8. Variation of impact strength with t_m for cryomilled h-PMMA (○), ambimilled h-PMMA (●) and cryomilled m-PMMA (△). The lines shown in this figure (solid for cryomilled samples and dashed for ambimilled samples) serve as guides for the eye. Error bars denote one standard deviation in the data.

dependence of T_g on $\bar{M}_n$ for milled h-PMMA and m-PMMA (l-PMMA is not included here due to the slight variation of T_g with t_m, <10°C, in Fig. 5) is evident in Fig. 7, in which T_g is presented as a function of $\bar{M}_n^{-1}$ for cryomilled h-PMMA (Fig. 7a), ambimilled h-PMMA (Fig. 7b) and cryomilled m-PMMA (Fig. 7c). According to each of these figures a simple linear relationship between T_g and $\bar{M}_n^{-1}$ does not accurately represent the data shown. Application of Eq. (2) to each of the data sets in Fig. 7 at short t_m, however, yields reasonable regressed fits from which values of T_g^∞ and α can be extracted. These constants are provided for comparison in Table 3 and, despite the highly nonequilibrium manner in which the homopolymers have been processed (in marked contrast to the highly controlled fractionation methods [29] used to obtain nearly monodisperse homopolymers of known $\bar{M}_n$), are in fair agreement with the values of T_g^∞ and α reported [31,32] elsewhere: 114–125°C for T_g^∞ and $(0.94–3.4)\times10^5$ for α.

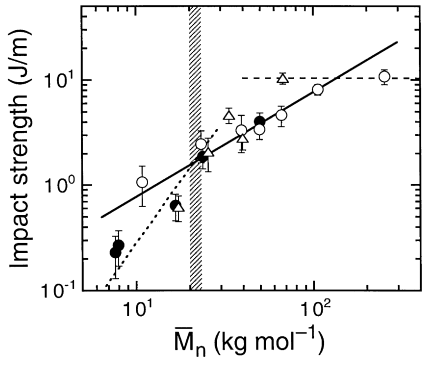

Fig. 9. Impact strength as a function of $\bar{M}_n$ on double-logarithmic coordinates illustrating the dependence of impact strength on $\bar{M}_n$ for cryomilled h-PMMA (○), ambimilled h-PMMA (●) and cryomilled m-PMMA (△). At high $\bar{M}_n$, the impact strength is nearly independent of $\bar{M}_n$ (dashed line). At lower $\bar{M}_n$, impact strength varies almost linearly with $\bar{M}_n$ (solid line). At $\bar{M}_n$ below M_0 (the range of M_0 is shown by the shaded area), the impact strength decreases abruptly (dotted line) due to insufficient molecular entanglement. Error bars denote one standard deviation in the data.

Such agreement regarding T_g^∞ is surprising, especially because high-energy mechanical milling initially tends to produce very broad molecular weight distributions (see Table 2), which can have a tremendous effect on the measured value of T_g [32]. The consistently higher values of α obtained here indicate that the T_g of milled PMMA is more sensitive to $\bar{M}_n$ than monodisperse PMMA fractions. While the data in Fig. 7 have been examined by established means (Eq. (2)) to glean insight into the relationship between T_g and $\bar{M}_n$ in mechanically milled PMMA, such analysis is plainly incapable of fully describing this relationship. Examination of Fig. 7 reveals that, at long t_m and, hence, low $\bar{M}_n$, T_g appears to reach a limiting value, suggesting that the T_g in these milled PMMA grades is better represented by an expression similar to Eq. (1) than by Eq. (2). Regression of an exponential function of the form

$$T_g(M) = T_g^* + be^{-k'M} \tag{3}$$

to each of the data sets in Fig. 7 accurately reflects the experimental data in each case, although the precise physical meaning of the regressed parameters T_g^* and k' obtained upon doing so is not clear. It is interesting to note that the values of k' derived for cryomilled h-PMMA (Fig. 7a) and m-PMMA (Fig. 7c) are comparable in magnitude: 0.89 and 0.94 mol kg^{-1}, respectively. Recall that similar agreement exists for the molecular-weight degradation constant (k) in Table 3.

One final factor that has been ignored in the present analysis is the dependence of T_g on PMMA tacticity. Tacticity alone can be responsible for differences of ca. 75°C in the reported [32] value of T_g^∞. No effort has, however, been made here to discern the initial tacticity of the PMMA grades used in the present study. Milling-induced chemical modification of macromolecules certainly constitutes an important topic for future investigation in the present vein.

3.3. Impact strength

To establish the effect of mechanical milling on the physical properties of PMMA, impact testing has been performed on specimens before and after milling. Results of these tests are displayed in Fig. 8 for h-PMMA (cryomilled and ambimilled) and m-PMMA (data for the l-PMMA grade could not be obtained due to insufficient sample cohesion upon melt pressing). Both as-received PMMA grades possess an impact strength of about 11 J m^{-1}, which compares favorably with values reported elsewhere [30,33] for PMMA, typically 10–16 J m^{-1}. As anticipated from the degradation in $\bar{M}_n$ observed in earlier sections, mechanical milling induces a dramatic reduction in impact strength. According to the data in Fig. 8, the impact strength of cryomilled h-PMMA is the least affected by milling when $t_m < 8$ h. The impact strength decreases to about 4 J m^{-1} after 3.5 h of cryomilling and falls below 2 J m^{-1} after 10 h of milling. More pronounced reductions in impact strength (to below 1 J m^{-1} after 5 h of milling) are realized in both the

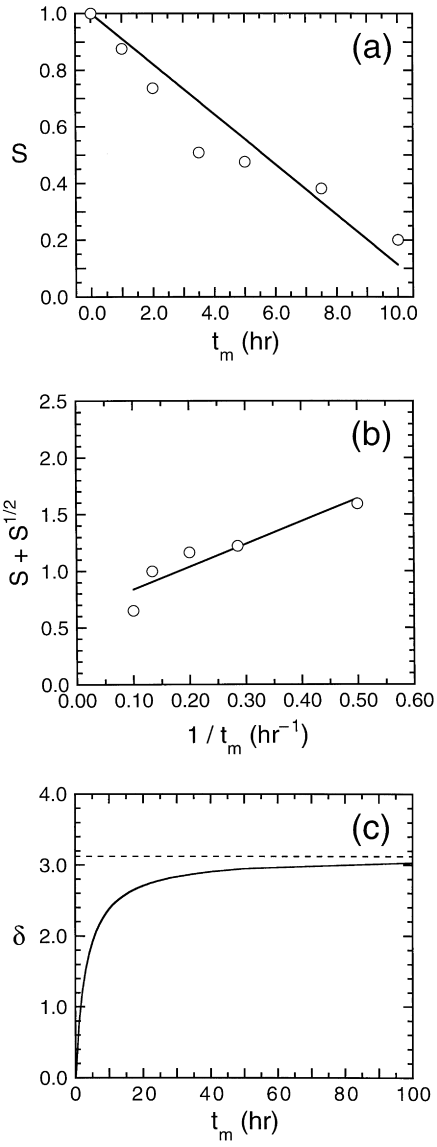

Fig. 10. Results from the sol–gel analysis of cryomilled PI. In (a), the soluble PI fraction (S) is shown as a function of t_m, with the solid line provided as a linear least-squares fit to the data. In (b), a Charlesby–Pinner plot showing the dependence of $S + S^{1/2}$ on t_m^{-1} for long t_m is displayed. A linear fit of these data to Eq. (4) yields the fracture and crosslinking densities per unit t_m. These parameters can be used to determine the crosslinking coefficient (δ), included as a function of t_m (solid line) in (c). The dashed line in (c) represents the value of δ in the limit as $t_m \rightarrow \infty$.

ambimilled h-PMMA and cryomilled m-PMMA specimens. Such discouraging performance is consistent with the fact that PMMA is a very brittle thermoplastic and is highly susceptible to mechanical damage [21,34].

The reduction in impact strength of mechanically milled PMMA is attributed to the accompanying decrease in molecular weight, since prior studies [27,35–39] have demonstrated that the strength and impact resistance of thermoplastics depend sensitively on molecular weight. Fig. 9 shows the variation of impact strength with $\bar{M}_n$ for all of the milled specimens included in Fig. 8 and confirms that the impact strength of milled PMMA depends on $\bar{M}_n$. Previous efforts have identified three distinct regions describing the molecular weight dependence of impact strength. At high molecular weights ($\bar{M}_n > 150$ kg mol^{-1} for PMMA [27]), impact strength is virtually independent on $\bar{M}_n$. Below this threshold, impact strength has been found to vary almost linearly with $\bar{M}_n$. The third detected regime occurs at $\bar{M}_n < M_0$, where M_0 is marginally less than M_c (M_0 has been measured [27,36,39] between 20 and 23 kg mol^{-1}). Within this regime, little if any impact strength can be measured due to insufficient molecular entanglement. While the impact strength data collected here exhibit experimental scatter, at least some of these features are present in Fig. 9.

As illustrated by the dashed horizontal line in Fig. 9, impact strength does not appear to be strongly dependent on $\bar{M}_n$ at high $\bar{M}_n$. At lower $\bar{M}_n$, impact strength is accurately described by a linear dependence on $\bar{M}_n$ (shown by the solid line in Fig. 9). The intersection between the horizontal line at high $\bar{M}_n$ and the regressed linear fit at intermediate $\bar{M}_n$ occurs at about 135 kg mol^{-1} (which is in reasonably good agreement with 150 kg mol^{-1} from Ref. [27]). Below the M_0 range, impact strength no longer decreases linearly with $\bar{M}_n$ but instead scales as $\bar{M}_n^{1.7}$ (dashed line in Fig. 9). In this case, the intersection between the linear fit at intermediate $\bar{M}_n$ and the power-law fit at low $\bar{M}_n$ ($<M_0$) occurs at about 21 kg mol^{-1}, which corresponds, within reported values, to M_0 of PMMA. Thus, the data in Fig. 9 dictate that $\bar{M}_n$ of mechanically milled PMMA cannot drop below M_0 if reasonable fracture resistance is desired. These data likewise provide a measure by which the upper limit on t_m (7.5 h for cryomilled h-PMMA and 10 h for m-PMMA) can be ascertained.

3.4. Chemical interactions

A sol–gel analysis has been performed to quantitate the fraction of milling-induced insoluble PI. The soluble fraction (S) of PI discerned from this analysis is presented as a function of t_m in Fig. 10. This graph verifies that the as-received PI is completely soluble in toluene, since no polymer is retained in the filter paper. After cryomilling for just for 1 h, however, a nontrivial fraction of insoluble PI is retained, increasing with an increase in t_m. This trend clearly indicates that PI undergoes interchain crosslinking during high-energy mechanical milling, and likewise explains the measured increase in the T_g of milled PI: crosslinking decreases the free volume of neighboring chains and increases the observed T_g.

The molecular evolution of PI during cryomilling can be more clearly elucidated in terms of a Charlesby–Pinner analysis. This treatment, originally developed as a means to explore the effect of radiation on polymers, relates exposure dose to radiation-induced molecular changes in polymers, such as crosslinking [40–43]. It relies on the presumption that crosslinking and chain scission occur

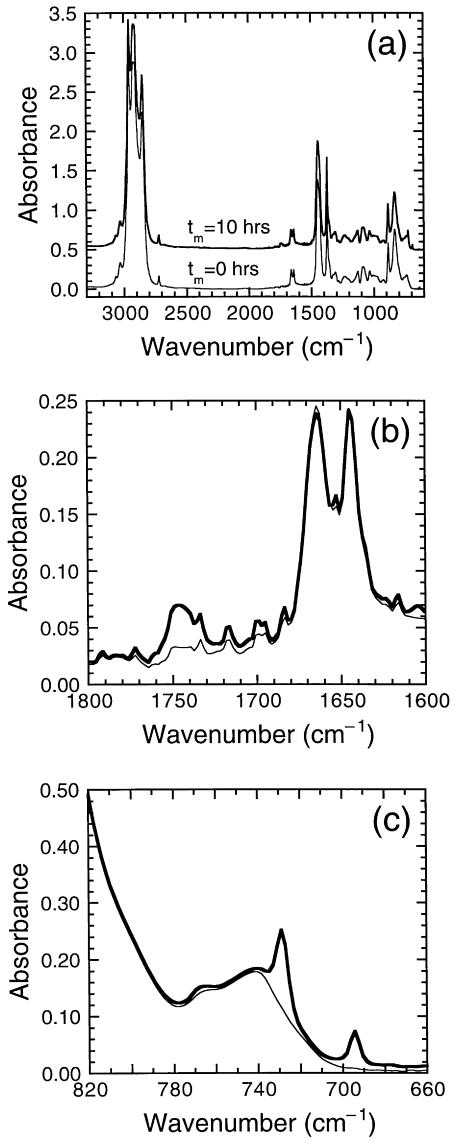

Fig. 11. FTIR spectra of cryomilled PI at t_m of 0 h (thin line) and 10 h (thick line). Full spectra are shown in (a), whereas (b) and (c) display enlargements of intervals in which differences between the two samples are evident. Peak assignments are discussed in the text.

simultaneously at random throughout the polymer, a condition that is believed to be sufficiently satisfied during high-energy mechanical milling. The relationship between S and dose (r) for a polymer possessing a random initial molecular weight distribution (PDI = 2.0) is given by [41]

$$S + S^{1/2} = \frac{2}{\delta} = \frac{p}{q} + \frac{1}{qNr} \tag{4}$$

where δ is the number of crosslinks per initial weight-average molecule, q represents the crosslink density per unit radiation dose, p is the fracture density per unit radiation dose and N denotes the number-average degree of polymerization. For other, non-random molecular weight distributions, Eq. (4) may be employed if r, and the number of chain scission events, is sufficiently high, in which case the molecular weight distribution can be considered nearly random.

To deduce the crosslinking coefficient (δ) promoted by mechanical milling, r in Eq. (4) is replaced by its mechanical analog (t_m). Shown in Fig. 10b is the dependence of $(S + S^{1/2})$ on t_m^{-1} at "long" t_m (2–10 h). A linear least-squares fit of the data in Fig. 10b yields $p/q = 0.64$ and $1/qN = 2.00$. Incorporating these values into Eq. (4) results in the time-dependent δ provided in Fig. 10c. Note that the value of δ at infinite t_m is also identified in this figure. Calculation of N (= 1012 from GPC analysis) reveals that q and p are equal to 4.9×10^{-4} and 3.2×10^{-4}, respectively. These values, which are dependent on milling conditions, indicate that chemical crosslinking is more likely (by about 50%) than scission during PI cryomilling. Determination of these Charlesby–Pinner parameters permits quantitation of the effects of high-energy mechanical milling on a crosslinkable polymer such as PI.

If sufficiently numerous, specific chemical changes in the cryomilled polymers examined here can be identified by FTIR spectroscopy. While no discernible changes are observed in the milled PMMA and PEP specimens, unmistakable FTIR spectral changes are detected in the milled PI samples. The FTIR spectra presented in Fig. 11a, offset to facilitate comparison correspond to PI in the as-received state ($t_m = 0$ h) and after cryomilling for 10 h. The principal features in the spectra identically match those reported in previous works, and the peak assignments are provided elsewhere [44]. Close examination of these spectra reveals milling-induced differences in the vicinity of 700 and 1750 cm^{-1}. Enlargements of these regions (without signal offset) are shown in Fig. 11b and c and confirm the existence of three small peaks (at 1745, 729 and 694 cm^{-1}) that are present in the cryomilled sample but not in the virgin PI. To properly assign these new absorbance peaks, we first examine the chain fracture process and subsequent reaction pathways of radicals produced in previous studies [45,46] of PI degradation.

The CH_2–CH_2 bond has been found to be the weakest bond in PI and is prone to rupture under mechanical stress. Chain scission at this bond is depicted in Scheme 1, in which a PI chain (**a**) is divided to form the radicals (**b**) and (**c**). These radicals may undergo resonance stabilization to form (**d**) and (**e**) and subsequently react, depending on milling conditions. In the absence of oxygen, three reaction pathways have been identified. The first of these involves the recombination of radicals (**b**) and (**c**) to reform a virgin PI chain. Another possibility is that the radicals react with an unsaturated bond of another molecule and form a crosslink (**f**), which can lead to the formation of a permanent network or gel. The last possibility is that an original radical (**c**) recombines with a resonance-stabilized radical (**d**) to form a PI chain with a pendant vinyl group (**g**). This reaction, only observed in high-purity Ar, is effectively prevented [45] in the presence of either N_2 or O_2. In the presence of oxygen, PI radicals react rapidly with O_2 molecules to produce peroxy

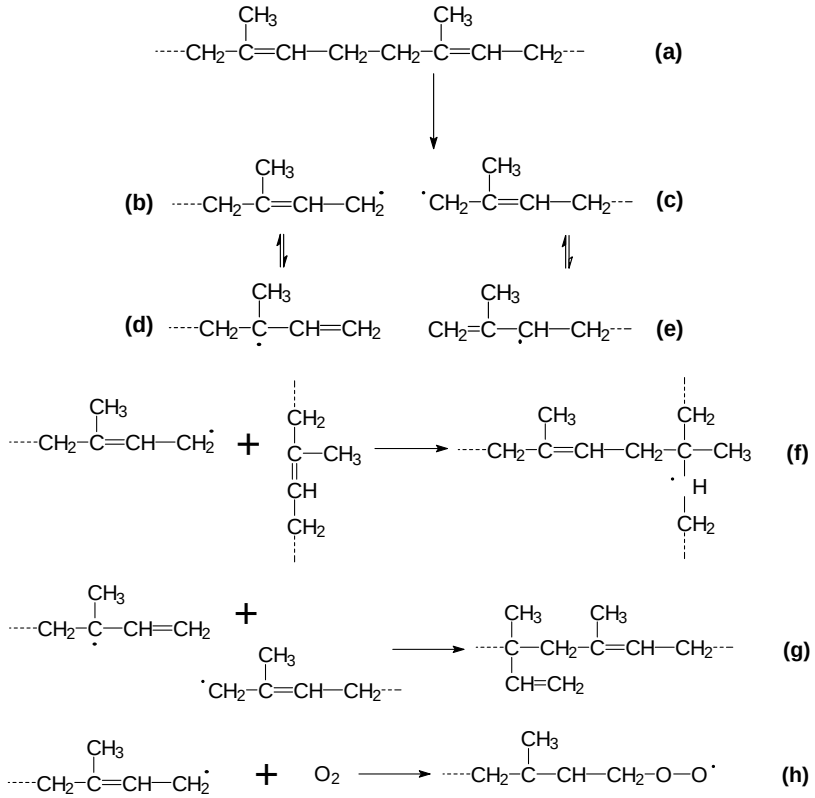

Scheme 1.

radicals (**h**), which may subsequently extract hydrogen from other molecules. If hydrogen is extracted from other PI molecules, further crosslinking will ensue.

On the basis of these possible reaction pathways, as well as prior FTIR assignments [47,48], the absorbance peaks produced during the cryomilling of PI (see Fig. 11b and c) are assigned the following vibration modes. The peak located at 694 cm^{-1} is attributed to the CH wag in the pendant vinyl group. The peak at 729 cm^{-1} may be associated with activation of the *cis*-CH wag of R-CH=CH-R groups due to nearby chain scission that occurs during milling, or the CH_2 rock of the molecules activated by the formation of either (i) $(CH_2)_3$–CH_3 groups via chain decomposition [47] or (ii) PI crystals [48] due to mechanical milling. (Such induced crystallization has been previously observed [45] during the mastication of natural rubber.) The excitation observed at 1745 cm^{-1} is sufficiently broad to accommodate several different molecular excitations that all involve oxygen [47,49–52]. Since milling is conducted in the absence of O_2, the presence of O_2 in the cryomilled PI FTIR spectrum strongly suggests the residual free radicals produced during milling react with atmospheric O_2 upon sample removal from the milling vial.

One final observation warranting discussion at this juncture is that the chemical crosslinking of PI, as well as the rapid molecular-weight reduction of PMMA and slower deterioration of PEP, during high-energy ball milling are remarkably consistent with the response of these materials to high-energy radiation [43,53]. Moreover, PET has been found [25,54] to be chemically resistant to mechanical milling and radiation exposure, both of which promote solid-state amorphization in metallic alloys [55,56]. A general correlation between the high-energy mechanical milling and irradiation of polymeric materials would permit use of the established body of work on polymer radiation damage to predict suitable polymer candidates that would be most resistant to milling-induced molecular modification.

4. Conclusions

In this study, three different polymers—PMMA, PI and PEP—have been subjected to high-energy mechanical milling to investigate their response to this solid-state processing technique. Results obtained here clearly demonstrate that mechanical milling of PMMA yields a substantial reduction in molecular weight, with larger chains breaking preferentially. In the case of polymers with an initial molecular weight above the critical molecular weight of entanglement, a lower molecular-weight limit (near the entanglement molecular weight) is identified below which chain scission proceeds very slowly. This behavior is consistent with the degradation of PMMA under mechanical strain [21,22], but occurs at a much higher rate due to the more vigorous action of milling. Accompanying the milling-induced decrease in molecular weight are reductions

in both the glass transition temperature and impact strength of PMMA. The dependence of impact strength on molecular weight varies with molecular weight regime, with the impact strength becoming negligibly small as the molecular weight is reduced below the chain entanglement limit. The value of this limiting molecular weight is estimated from the results acquired here to be about 21 kg mol^{-1}. Moreover, milling performed at ambient temperature more severely degrades the molecular weight of PMMA than milling conducted at cryogenic temperatures. This observation is attributed to the increase in atomic thermal vibrations, which augment chain scission, by mechanical strain.

For the PI and PEP, the effects of cryogenic mechanical milling depend strongly on polymer type. Mechanical milling of saturated PEP results in monotonic reductions in molecular weight and glass transition temperature. Relative to PMMA, however, the rate of molecular weight degradation is much slower, and a narrowed molecular weight distribution is not observed. The unsaturated PI exhibits a substantially different response to mechanical milling than does PEP. Crosslinking of PI chains yields an insoluble fraction that increases with increasing milling time. Corresponding glass transition temperature measurements show a large initial decrease, followed by almost complete recovery due to chemical crosslinking. Crosslinking analysis based on the Charlesby–Pinner treatment developed for radiation-induced scission/crosslinking indicates that: (i) 2.4 crosslinks per initial weight-average molecule form after 10 h of milling; and (ii) crosslinking is 1.5× more likely than chain scission for PI during mechanical milling. Spectroscopy of milled PI reveals three milling-induced peaks, which confirm the formation of new chemical bonds during milling. These results demonstrate that the effect of high-energy mechanical milling on polymers can be profound. While solid-state mechanical milling holds the promise of yielding nanoscale-mixed polymer blends from two or more chemically dissimilar macromolecules [57–59], milling-induced changes in molecular structure and chemistry, such as those identified here, must be considered carefully if this strategy is to be explored as a viable processing technology.

Acknowledgements

Support for A.P.S. and H.A. has been provided by the National Science Foundation through Young Investigator Award DMR-945-8060. We thank Dr B.-S. Chiou and Mr A.G. Erlat for technical assistance.

References

[1] Utracki LA. Polymer alloys and blends. Berlin: Hanser, 1990.
[2] Sperling LH. Polymeric multicomponent materials. New York: Wiley, 1997.
[3] Macosko CW, Guegan P, Khandpur AK, Nakayama A, Marechal P, Inoue T. Macromolecules 1996;29:5590.
[4] Lyatskaya Y, Gersappe D, Balazs AC. Macromolecules 1995; 28:6278.
[5] Feng Y, Weiss RA, Han CC. Macromolecules 1996;29:3925.
[6] Bouilloux A, Ernst B, Lobbrecht A, Muller R. Polymer 1997;38:4775.
[7] Pan J, Shaw WJD. Microstructural Sci 1993;20:351.
[8] Pan J, Shaw WJD. Microstructural Sci 1994;21:95.
[9] Farrell MP, Kander RG, Aning AO. J Mater Synth Proc 1996;4:1996.
[10] Font J, Muntasell J, Cesari E. Mater Res Bull 1999;34:157.
[11] Ishida T. J Mater Sci Lett 1994;13:623.
[12] Ahn D, Khait K, Petrich MA. J Appl Polym Sci 1995;55:1431.
[13] Nesarikar AR, Carr SH, Khait K, Mirabella FM. J Appl Polym Sci 1997;63:1179.
[14] Koch CC. In: Cahn RW, editor. Materials science and technology, 15. Weinheim: VCH, 1991.
[15] Benjamin JS. Metall Trans 1970;1:2943.
[16] Lu L, Lai MO. Mechanical alloying. Dordrecht: Kluwer Academic, 1998.
[17] Murty BS, Ranganathan S. Int Mater Rev 1998;43:101.
[18] Pan J, Shaw WJD. Microstructural Sci 1992;19:659.
[19] Shaw WJD, Pan J, Growler MA. In: DeBarbadillo JJ, Fores FH, Schwarz R, editors. Proc Second Int Conf Struct Appl Mech Alloying, Materials Park, OH: ASM International, 1993.
[20] Castricum HL, Yang H, Bakker H, Deursen JHV. Mater Sci Forum 1997;235–38:211.
[21] Baramboim NK. In: Watson WF, editor. Mechanochemistry of polymers, London: MacLaren and Sons, 1964.
[22] Casale A, Porter RS, Johnson JF. Rubber Chem Tech 1971;4:534.
[23] Sohma J. Prog Polym Sci 1989;14:451.
[24] Kausch HH. Polymer fracture. 2. New York: Springer, 1987.
[25] Bai C, Spontak RJ, Koch CC, Saw CK, Balik CM. Submitted for publication.
[26] Matsuoka S. Relaxation phenomena in polymers. Munich: Hanser, 1992.
[27] Young RJ. In: Booth C, Price C, Price C, editors. Comprehensive polymer science: the synthesis, characterization, reactions and applications of polymers, 2. New York: Pergamon Press, 1989.
[28] Casale A. J Appl Polym Sci 1975;19:1461.
[29] Fox TG, Flory PJ. J Appl Phys 1950;21:581.
[30] Sperling LH. Introduction of physical polymer science. 2. New York: Wiley, 1992.
[31] Thompson EV. J Polym Sci A-2 1966;4:199.
[32] Ute K, Miyatake N, Hatada K. Polymer 1995;36:1415.
[33] Adams GC, Wu TK. In: Brostow W, Corneliussen RD, editors. Failure of plastics, Munich: Hanser, 1986.
[34] Porter RS, Casale A. Polym Eng Sci 1985;25:129.
[35] Vincent PI. Polymer 1960;1:425.
[36] Gent AN, Thomas AG. J Polym Sci A-2 1972;10:571.
[37] Martin JR, Johnson JF, Cooper AR. J Macromol Sci: Rev Macromol Chem C 1972;8:57.
[38] Nunes RW, Martin JR, Johnson JF. Polym Eng Sci 1982;22:205.
[39] Turner DT. Polymer 1982;23:626.
[40] Charlesby A, Pinner HS. Proc R Soc A 1959;249:367.
[41] Charlesby A. Atomic radiation and polymers. New York: Pergamon Press, 1960.
[42] Zaharescu T, Mihalcea I. Polym Degrad Stabil 1997;55:265.
[43] Dawes K, Glover LC. In: Mark JE, editor. Physical properties of polymers handbook, New York: AIP Press, 1996.
[44] Zhang R. In: Mark JE, editor. Polymer data handbook, New York: Oxford University Press, 1999.
[45] Ceresa RJ. Block and graft copolymers. Washington, DC: Butterworth, 1962.
[46] Schnabel W. Polymer degradation: principles and practical applications. Munich: Hanser, 1981.
[47] Colthrup NB, Daly LH, Wiberly SE. Introduction to infrared and Raman spectroscopy. 3. San Diego, CA: Academic Press, 1990.

[48] Gavish M, Brennan P, Woodward AE. Macromolecules 1988;21: 2075.
[49] Cook JW, Edge S, Packham DE, Thompson AS. J Appl Polym Sci 1997;65:1379.
[50] Kumar NR, Roy S, Gupta BR, Bhowmick AK. J Appl Polym Sci 1992;45:937.
[51] Poh BT, Lee KS. Eur Polym J 1994;30:17.
[52] Ivan G, Giurginca M. Polym Degrad Stabil 1998;62:441.
[53] Sawyer LC, Grubb D. Polymer microscopy. 2. London: Chapman and Hall, 1996.
[54] Rightor EG, Hitchcock AP, Ade H, Leapman RD, Urquhart SG, Smith AP, Mitchell G, Fisher D, Shin HJ, Warwick T. J Phys Chem B 1997;101:1950.
[55] Bellon P, Martin G. In: Yavari AR, editor. Ordering and disordering in alloys, London: Elsevier, 1992.
[56] Martin G, Bellon P. In: Schwarz RB, Johnson WL, editors. Solid state amorphizing transformations, Lausanne, The Netherlands: Elsevier Sequoia, 1988.
[57] Balik CM, Bai C, Koch CC, Spontak RJ, Saw CK. Mater Res Soc Symp Proc 1997;461:39.
[58] Smith AP, Bai C, Ade H, Spontak RJ, Balik CM, Koch CC. Macromol Rap Commun 1998;19:557.
[59] Smith AP, Spontak RJ, Ade H, Smith SD, Koch CC. Adv Mater 1999;11:1277.